The Simulation of East Asian Summer Monsoon Precipitation With a Regional Ocean-Atmosphere Coupled Model

Yongjiu Dai[1] 🔟, Haiqin Li[2], and Liqiang Sun[3]

[1]School of Atmospheric SciencesSun Yat-sen University, Guangzhou, China, [2]University of Colorado CIRES at the NOAA ESRL/Global Systems Division, Boulder, CO, USA, [3]North Carolina Institute for Climate Studies, North Carolina State University, Raleigh, NC, USA

Abstract A fully coupled regional ocean-atmosphere model was used to simulate the East Asian summer monsoon (EASM) precipitation. This coupled regional climate modeling system consists of the Regional Spectral Model (RSM) for the atmosphere and the Regional Ocean Modeling System for the ocean. The ocean and atmosphere share the same horizontal grid resolution. The coupled model is forced by the National Centers for Environmental Prediction-Department of Energy (R-2) global atmospheric reanalysis and Simplified Ocean Data Assimilation global oceanic reanalysis through the lateral boundary. This study examines EASM surface oceanic state and precipitation variability from a 22-year (1984–2005) integration with a horizontal resolution of 40 km. The coupled model captures the features of observed sea surface temperature (SST), sea surface height, and ocean surface currents. Compared with the control run of the uncoupled RSM forced with observed SSTs, the coupled model shows more realistic simulation of the EASM precipitation climatology. The coupled model also improves the simulation of precipitation variability at both interannual and intraseasonal scales. It is the coupled model, not the uncoupled RSM, represents the observed SST-precipitation and SST-evaporation relationships. This study indicates that the ocean-atmosphere coupling is essential for model simulations of the EASM precipitation.

1. Introduction

East Asia summer monsoon (EASM) covers a vast region of East Asian continent and the western North Pacific (WNP) in the midlatitudes and the subtropics. It is a key part of the Asian summer monsoon system (Ding & Chan, 2005). Southerly winds of EASM carry warm and moist air from the South China Sea, Indian, and Pacific Oceans and bring water to East Asia. The anomalous monsoon precipitation often causes flooding or drought, which has great economic and social impacts in East Asia. The atmosphere, land, and the ocean are a coupled system, exchanging heat, momentum, and water at the air-land and air-sea interfaces. In general, in the summer the atmosphere receives heat from the ocean, thus affecting the atmospheric circulation and surface winds, which in turn generate ocean currents and the large-scale ocean circulation. The air-sea interaction is also very active, and many extreme precipitation events are observed within the EASM system (Kim & Hong, 2010).

Numerical models have been extensively used for climate studies of the EASM. Wang et al. (2004) used multiple Atmosphere General Circulation Models (AGCMs) to investigate the Asian-Australian monsoon variability. The observed boreal summer SST-precipitation correlation is negative over East Asia, while this correlation in AGCM simulations is positive. The misrepresentation of SST-precipitation relationship in AGCMs is attributed to the lack of ocean-atmosphere coupling. The studies from Zhou et al. (2009) and Song and Zhou (2014) find that SST-driven standalone AGCM simulations show some skills in the simulation of interannual boreal summer precipitation variability over the Asian-Australian monsoon region due to the remote SST anomaly (SST) forcing associated with El Niño–Southern Oscillation, but local SST bias in the western Pacific indeed has caused bias in the simulation of precipitation change as reported previously. Wu and Kirtman (2007) carried out a study on regimes of seasonal air-sea interaction and suggested that the performance of atmospheric general circulation model simulations forced by observed SST is closely linked to the regime of air-sea interaction: The forced simulations have good performance when SST forcing dominates, and the performance is low or poor when atmospheric forcing dominates. Lack of ocean-atmosphere coupling has been regarded as the key factor contributing to the poor simulation of precipitation over the EASM region (Zhou et al., 2009).

Table 1
RSM Physics

	Parameterization	References
Deep convection	Kain and Fritsch	Kain (2004)
Shallow convection	Tiedtke scheme	Tiedtke (1983)
Boundary layer	Nonlocal scheme	Hong and Pan (1996)
Longwave radiation	M.-D. Chou	Chou and Suarez (1994)
Shortwave radiation	M.-D. Chou	Chou and Lee (1996)
Cloud	Slingo	Slingo (1987)
Gravity wave drag	Pierrehumbert	Alpert et al. (1988)
Land model	NOAH LSM	Ek et al. (2003)

Note. RSM = Regional Spectral Model; LSM = land surface model.

A most recent review (Gorgi & Gao, 2018) also highlights the importance of coupling different Earth components, including the ocean, to form the Regional Earth System Model. There have been a growing number of attempts recently to apply regional air-sea coupled models for the EASM region. The sensitivity of the model's behavior to air-sea coupling in different regional models was examined in case studies and demonstrated the importance of air-sea coupling for EASM simulation (Fang et al., 2010; Ren & Qian, 2005). Kim and Hong (2010) incorporated a mixed layer ocean model into the Weather Research and Forecasting model over East Asia and found that the inclusion of the ocean mixed layer model resulted in the reduction of systemic biases of excessive precipitation and weakening of the North Pacific high in the summer climate. Cha et al. (2016) showed that the Seoul National University Regional Climate Model coupled with a slab ocean model can improve rainfall-SST correlation over the tropical WNP around the Philippines and over the ocean surrounding Korea Peninsula. Zou and Zhou (2013) evaluated a regional coupled model (i.e., Flexible Regional Ocean Atmosphere Land System) in simulation of interannual variability of rainfall in WNP. Compared with the uncoupled simulation, the regionally coupled simulation exhibits improvements in both the climatology and the interannual variability of rainfall over the WNP.

A fully coupled regional ocean-atmosphere modeling system of Regional Spectral Model (RSM)-Regional Ocean Modeling System (ROMS) was developed recently. The RSM (Juang et al., 1997; Juang & Kanamitsu, 1994; Kanamitsu et al., 2010) is used for the atmosphere part, and the ROMS (Shchepetkin & McWilliams 2003) is applied for the ocean part. The RSM and ROMS are designed to share the same domain and resolution in the regional coupled modeling system, thus to eliminate the interpolation of coupling fields from source grid to target grid in most regional coupled models. This RSM-ROMS coupled modeling system has been successfully used in the 10-km downscaling of global reanalysis and regional climate change projection over California Current System. The coupled downscaling well resolves the costal upwelling and significantly impacts the costal mesoscale circulation of Catalina eddy. The much more realistic ocean and atmospheric states from the coupled downscaling indicate the importance of ocean-atmosphere interactions over California (Li et al., 2012; Li, Kanamitsu, Hong, Yoshimura, Cayan, & Misra, 2014; Li, Kanamitsu, Hong,
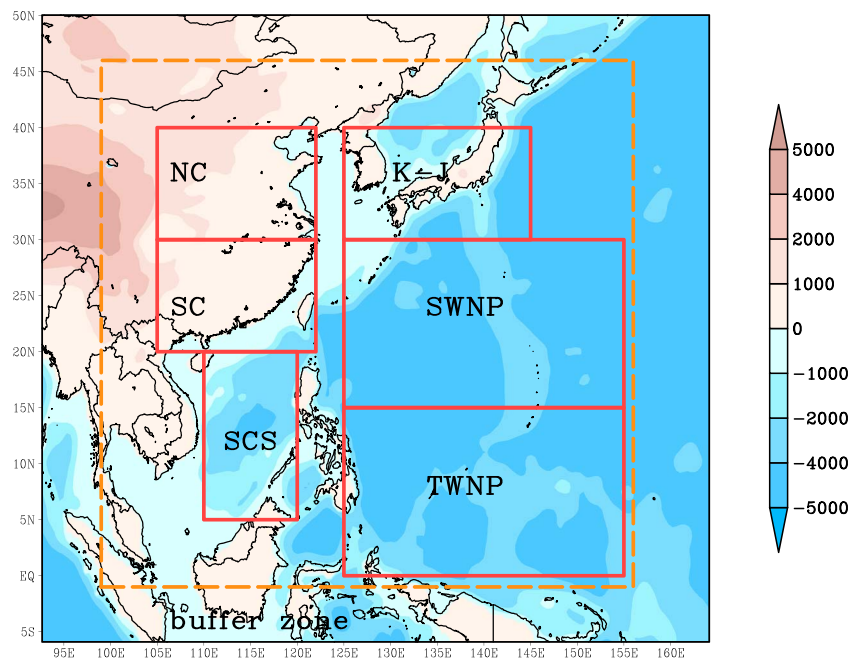

Figure 1. Model domain, topography, and bathymetry (m). The regions of northern part of China (NC), southern part of China (SC), South China Sea (SCS), Korea-Japan (K-J), subtropical Western North Pacific (SWNP), and tropical Western North Pacific (TWNP) are used for the subsequent analysis.
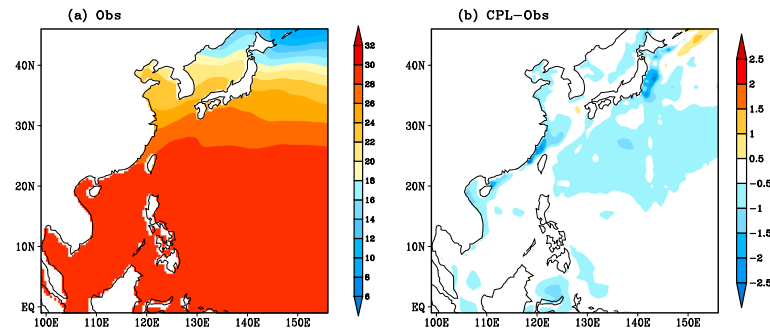
Figure 2. (a) Observed JJA SST climatology for the period of 1986–2005, and (b) bias of JJA SST climatology from the CPL. Unit is in degrees centigrade (°C). SST = sea surface temperature; JJA = June-July-August.

Yoshimura, Cayan, Misra, & Sun, 2014). The RSM-ROMS has also been applied over the Intra-American Seas at 15-km resolution, and it well simulated the loop current and the episodic loop current eddy, while the loop currents and eddy are rather poorly resolved in the Climate Forecast System Reanalysis (Li & Misra, 2014). It also improves the simulation of costal precipitation, heat flux, and surface air temperature around Japan compared with the uncoupled runs (Ham et al., 2016).

In this study, we investigate the ocean-atmosphere coupling impact on the EASM precipitation climatology and precipitation variability in interannual, intraannual, and intraseasonal scales with the fully coupled RSM-ROMS. The description of the coupled model and the experiments are introduced in section 2. The simulated surface oceanic state is described in section 3. In section 4, the simulated EASM precipitation is examined. The discussions and conclusions are given in sections 5 and 6, respectively.

2. Description of Model and Experiments

2.1. The Regional Ocean-Atmosphere Coupled Model

The atmospheric component of this fully coupled regional ocean-atmosphere modeling system, RSM-ROMs, is the RSM (Juang et al., 1997; Juang & Kanamitsu, 1994; Kanamitsu et al., 2010), which is a primitive equation regional atmospheric model. The RSM uses a spectral method with sine and cosine series in zonal and meridional dimensions (Juang & Kanamitsu, 1994). The RSM physical schemes used for CPL and UNCPL are listed in Table 1. It includes the cloudiness (Slingo, 1987), longwave (Chou & Suarez, 1994) and shortwave radiation (Chou & Lee, 1996), the updated Kain-Fritsch convective parameterization scheme (Kain, 2004) for deep convection, a nonlocal boundary layer scheme (Hong & Pan, 1996), and the four-layer community Noah land surface model (Ek et al., 2003). A spectral nudging method of scale-selective bias correction (Kanamaru & Kanamitsu, 2007, Kanamitsu et al., 2010) is also used to prevent large-scale atmospheric drift during the model integration.

Figure 3. Observed and CPL-simulated JJA SST anomalies (°C) over (a) South China Sea (SCS), (b) subtropical western North Pacific (SWNP), and (c) tropical western North Pacific (TWNP). SST = sea surface temperature; JJA = June-July-August.

The oceanic component of RSM-ROMS is the ROMS (Haidvogel et al., 2000; Shchepetkin & McWilliams 2003), which is a free surface, terrain-following, primitive equation regional ocean model. It was further developed from the S-coordinate Rutgers University Model (Song & Haidvogel, 1994). ROMS includes accurate and efficient physical and numerical algorithms, such as high-order advection schemes (Shchepetkin & McWilliams, 1998); accurate pressure gradient algorithms (Shchepetkin & McWilliams, 1998); several subgrid-scale parameterizations (Haidvogel & Beckmann, 1999); atmospheric, oceanic, and benthic boundary layers (Large et al.,
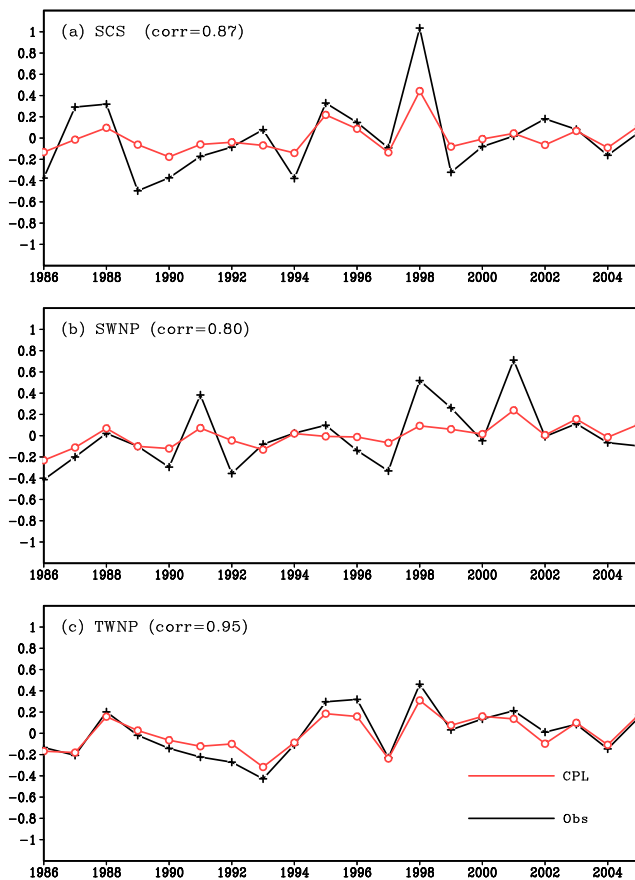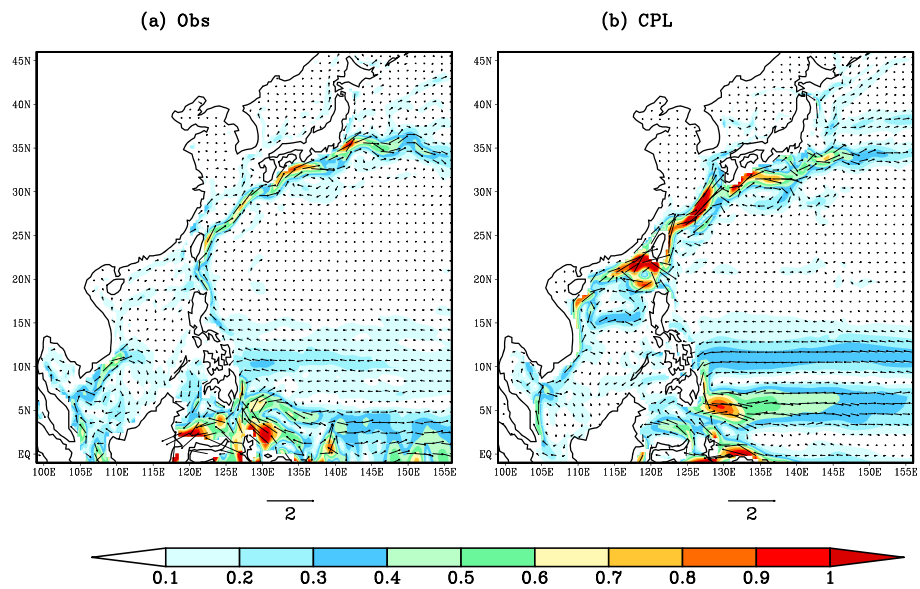
Figure 4. The ocean surface current JJA climatology (m/s) from (a) OSCAR satellite observation, and (b) CPL simulation. SST = sea surface temperature; JJA = June-July-August; OSCAR = Ocean Surface Current Analysis Real time.

1994); biological modules (Fasham et al., 1990); radiation boundary conditions (Marchesiello et al., 2001); and data assimilation (Fisher, 1998).

The RSM and ROMS are coupled in parallel with flexible coupling interval. The RSM and ROMS are designed to share the same domain and resolution in the regional coupled modeling system, and the SST-flux is directly exchanged between RSM and ROMS. The interpolation between atmosphere and ocean model grids is avoided, and a SST-flux coupler is not necessary. RSM-ROMS is designed for the practical application of the ocean-atmosphere coupled downscaling of global reanalysis (Ham et al., 2016; Li et al., 2012; Li & Misra, 2014), climate change projection (Li, Kanamitsu, Hong, Yoshimura, Cayan, & Misra, 2014; Li, Kanamitsu, Hong, Yoshimura, Cayan, Misra, & Sun, 2014), and seasonal prediction. Details of the regional coupled modeling system are referred to Li et al. (2012).

2.2. Experiments

An uncoupled experiment of RSM forced by prescribed SSTs was executed as a control run (UNCPL hereafter), and another experiment with the coupled model of RSM-ROMS (CPL hereafter) was also conducted. The
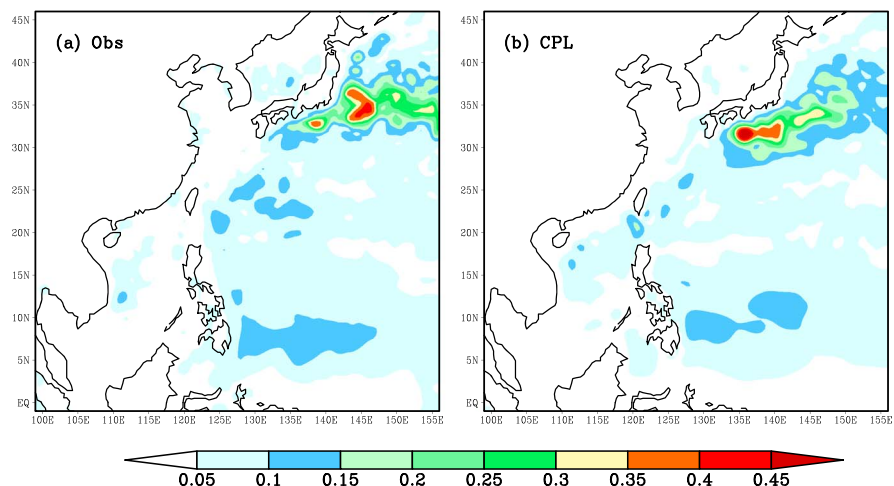

Figure 5. The standard deviation of sea surface height (SSH) for the period of JJA 1986–2005. (a) AVHRR observation and (b) CPL simulation. Unit is meter. JJA = June-July-August; AVHRR = Advanced Very High Resolution Radiometer.
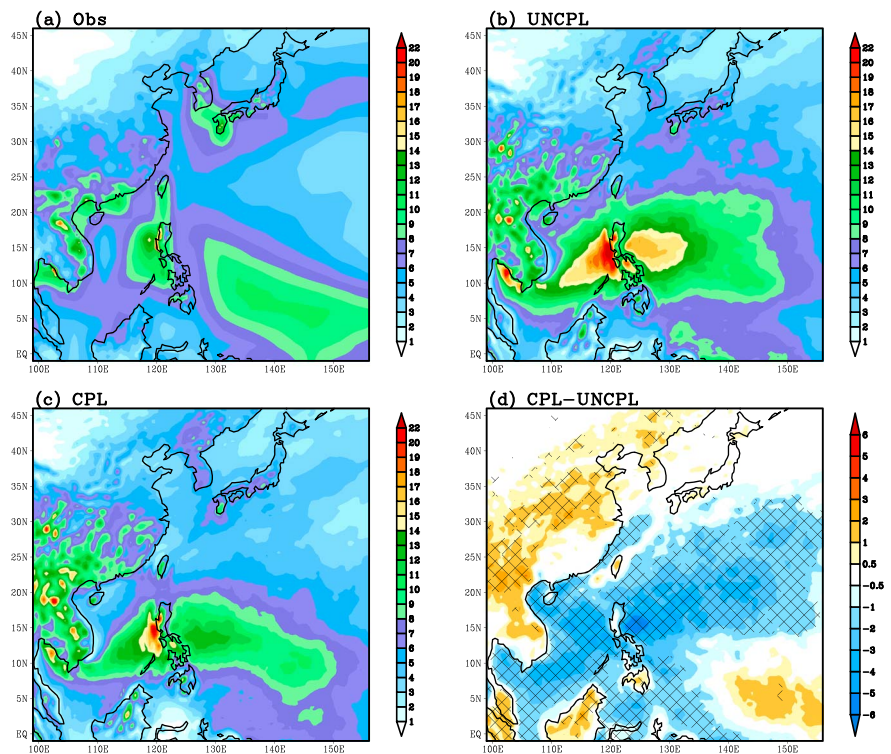
Figure 6. JJA precipitation climatology (mm/day) from (a) observation, (b) UNCPL, (c) CPL, and (d) CPL-UNCPL (color hatching indicates that the difference is statistically significant at 95% confidence level). JJA = June-July-August.

integration period of CPL and UNCPL is from 1984 to 2005. In order to account for sufficient spin-up of ocean, the first 2 years are discarded (Li et al., 2012). We will analyze the simulations for June-July-August (JJA) of the remaining 20 years (1986–2005) in this study.

The identical domain (5.415°S–50.334°N, 92.725°E–164.245°E) for UNCPL and CPL is shown in Figure 1. Six regions of tropical western North Pacific (TWNP), subtropical western North Pacific (SWNP), South China Sea (SCS), southern part of China (SC), northern part of China (NC), and Korea-Japan (K-J), as outlined in Figure 1 are used to analyze the SST and precipitation variability. There is an identical 40-km horizontal resolution for both RSM and ROMS in the CPL experiment. There are 28 vertical atmosphere sigma levels
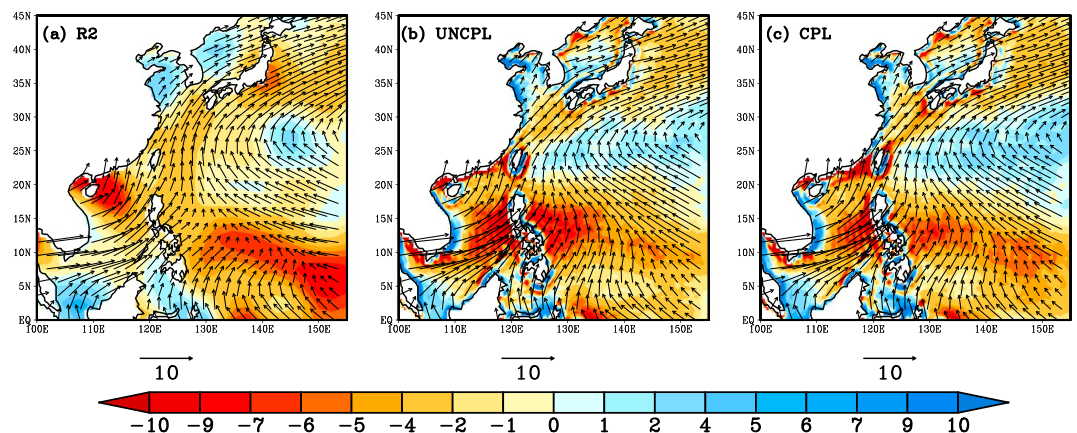

Figure 7. JJA climatology of 850-mb winds (m/s, vector) and 1,000-mb moisture flux convergence (10^{-4} s^{-1}g/kg, coloring) from (a) R2, (b) UNCPL, and (c) CPL. JJA = June-July-August.
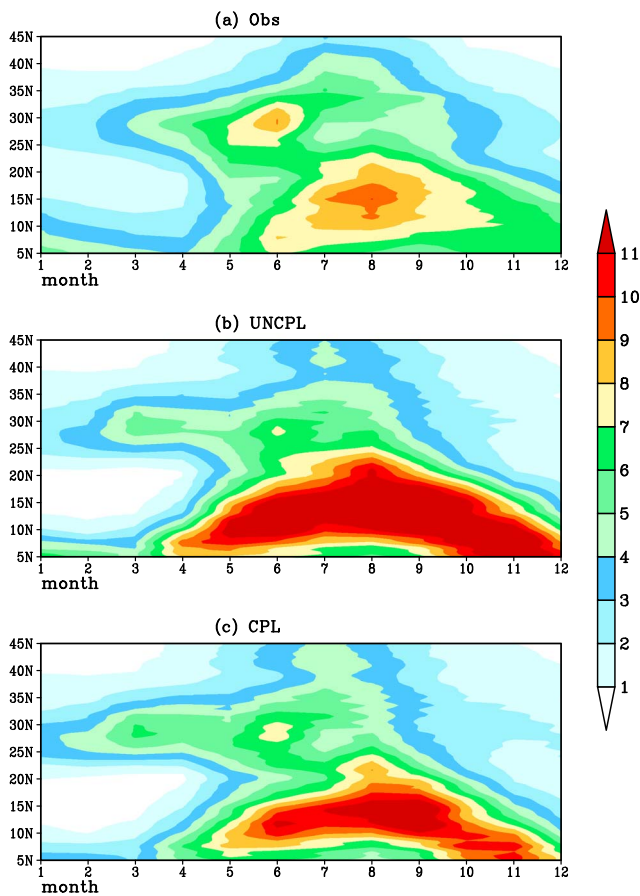
Figure 8. Monthly precipitation climatology (mm/day) averaged between 105°E and 140°E from (a) observation, (b) UNCPL, and (c) CPL.

for RSM. The T62 (~200 km) R2 Reanalysis (Kanamitsu et al., 2002) is used as atmospheric initial and boundary conditions.

The SST for the UNCPL run is from the daily Optimally Interpolated SST (OISST, Reynolds et al., 2007). The resolution of this SST data is 1° and will hereafter be referred to as the OISST. The oceanic initial and boundary condition for CPL is from the monthly Simple Ocean Data Assimilation (SODA, Carton et al., 2000). SODA is available at 0.5° horizontal resolution with 40 vertical layers and is interpolated to grids with 40-km horizontal resolution and 30 vertical oceanic sigma levels. A 6-hr coupling interval is employed in the CPL experiment. RSM offers atmospheric flux to ROMS and uses the SST from ROMS simulation. In order to reduce the large-scale SST bias in CPL, the monthly mean climatology OISST is used in the ROMS built-in correction scheme (Marchesiello et al., 2001) and leaves the freedom for SST anomaly developing.

2.3. Data Sets for Verification

The monthly Global Precipitation Climatology Project (GPCP, Huffman et al., 1997, available on 2.5° × 2.5°grid) over ocean and the Asian Precipitation - Highly Resolved Observational Data Integration Towards Evaluation (Yatagai et al., 2012, available on 0.25° × 0.25°grid) over land are used to validate the climatology, interannual, and intraannual variability of EASM precipitation. The daily GPCP precipitation data for the period of October 1996 to December 2005 are used to examine the intraseasonal variability of precipitation, and the resolution of daily GPCP data is in 1° × 1° grid (Huffman et al., 2001). The simulated cloud fraction is validated with the International Satellite Cloud Climatology Project (D2, Rossow & Schiffer, 1999).

The monthly mean SSTs, calculated from the daily OISST, are used to verify model-simulated SSTs. Noted that the daily OISST is also used to force the UNCPL. The sea surface height (SSH) is validated with the AVISO Altimetry (http://aviso.oceanobs.com), which is available from 1993 to present. The ocean surface current is validated with Ocean Surface Current Analysis Real time (Bonjean & Lagerloef, 2002), which is available from 1993 to present. All of these observational data were interpolated to 40-km model grid.

Table 2
The JJA Precipitation MBE (mm/day) and RMSE (mm/day) of the UNCPL and CPL Against the Observation (GPCP Over Ocean, APHRODITE Over Land)

	MBE		RMSE	
	UNCPL	CPL	UNCPL	CPL
NC	−0.52	0.32	0.70	**0.66**
SC	0.51	0.36	0.94	**0.69**
K-J	−1.48	−1.75	**1.67**	1.80
SCS	4.90	1.84	5.21	**2.46**
SWNP	2.74	0.56	2.94	**1.02**
TWNP	0.18	−0.34	1.76	**1.54**

Note. JJA = June-July-August; MBE = mean bias error; RMSE = root-mean-square error; GPCP = Global Precipitation Climatology Project; APHRODITE = Asian Precipitation - Highly Resolved Observational Data Integration Towards Evaluation; NC = northern part of China; SC = southern part of China; K-J = Korea-Japan; SCS = South China Sea; SWNP = subtropical western North Pacific; TWNP = tropical western North Pacific. Values in bold indicate better results.

3. The Simulation of Surface Oceanic State

The ocean-atmosphere interaction occurs at the ocean surface. The SST, SSH, and ocean surface currents are examined in this section.

3.1. Sea Surface Temperature

Figure 2a shows the observed June-July-August (JJA) SST climatology for the period of 1986–2005. There is a north-south SST gradient across the model domain. The CPL is able to produce this north-south JJA SST gradient (not shown). Figure 2b shows the JJA SST climatology bias from the CPL simulation. A cold bias prevails over most of the domain, particularly along the coastline of Vietnam, China, and Japan, and in SWNP. Cold bias in SWNP is also found in other coupled model simulations (Cha et al., 2016; Zou & Zhou, 2013). A possible explanation for this pervasive SST cold bias might be the excessive cloud cover in the CPL simulation. Compared with the International Satellite Cloud Climatology Project observation, our CPL generated excessive cloud cover in SWNP, which resulted
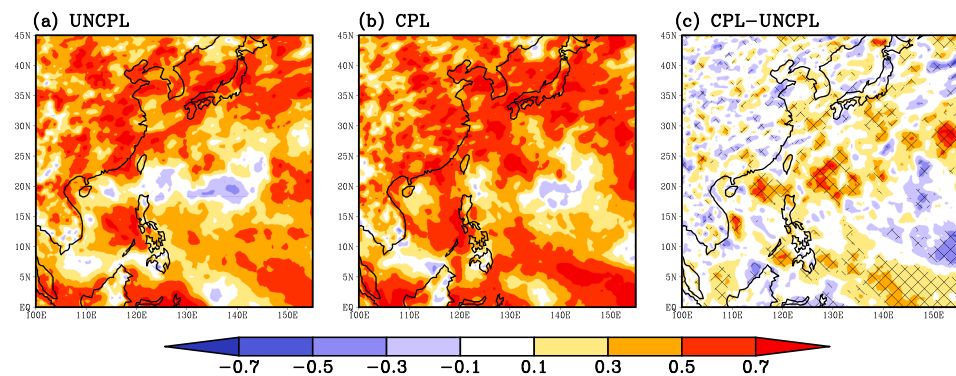
Figure 9. The correlation coefficients of JJA precipitation for the period of 1986–2005 between observation and (a) UNCPL, (b) CPL, and (c) CPL-UNCPL (color hatching indicates that the difference is statistically significant at 95% confidence level). JJA = June-July-August.

in less shortwave radiation at the ocean surface (not shown). An effort in further developing the cloud-radiation physics for ocean-atmosphere coupled modeling over East Asia is needed.

The observed and CPL-simulated JJA SST anomalies from over the regions of SCS, SWNP, and TWNP are shown in Figure 3. The CPL reproduces the JJA SST anomalies over SCS (Figure 3a) in most years, and the SST anomaly correlation against observation is 0.87 over SCS. Although the SST anomaly correlation is 0.80 over SWNP, the CPL-simulated variations are smaller than the observations. Note that the SST bias is large over SWNP, and the climatology heat flux correction may prevent the surface oceanic evolution over SWNP. The JJA SST anomaly variations over TWNP from the CPL match the observation well, and the correlation between them is as high as 0.95.

3.2. Ocean Surface Currents

Figure 4 shows the ocean surface currents JJA climatology for the period of 1986–2005. The Kuroshio Current, a strong western boundary current, begins off the east coast of Luzon, Philippines and Taiwan, flows northeastward past the East China Sea and Japan, and then out into the North Pacific (Figure 4a). The CPL generally reproduces the fast-moving narrow Kuroshio, although it is wider and stronger, particularly in the East China Sea. This may be attributed to the model relatively low resolution. Previous study indicated the model with high resolution can resolve the observed Kuroshio Current (Sakamoto et al., 2005).

3.3. Sea Surface Height

The standard deviation of the boreal summer SSH anomalies is shown in Figure 5. The variability of SSH is a reflection of the corresponding variability in the ocean circulation and ocean heat storage. The highest values are observed in the Kurishio Extension, where it is located off the east coast of Japan (Figure 5a). The Kuroshio extension forms a meandering boundary between the cold northern waters and the warm, southern, subtropical waters of the Pacific. The SSH difference across the width of the Kuroshio extension can be greater than a meter (Fearing et al., 2006). The vigorously meandering of the Kuroshio extension causes the large variability of SSH in this area. The CPL is able to capture this feature of SSH summer variability (Figure 5b).

4. The Simulation of EASM Precipitation

4.1. Climatology

The boreal summer precipitation climatology from observation, UNCPL, and CPL is shown in Figure 6. There is an observed northeastward rainfall band over SC, the Yangtze River basin, Korea, and Japan (Figure 6a). The monsoon advances northward and induces the heavy precipitation of Meiyu, Changma, and Baiu in China, Korea, and Japan, respectively (Ding & Chan, 2005). There is another observed southeastward rainfall band focused on the Indochina peninsula, the eastern SCS, the Philippines, and the TWNP (Figure 6a). Both UNCPL (Figure 6b) and CPL (Figure 6c) produce a northeastward rainfall band over SC, the Yangtze River basin, Korea, and Japan and underestimate the precipitation over K-J. The UNCPL overestimates precipitation
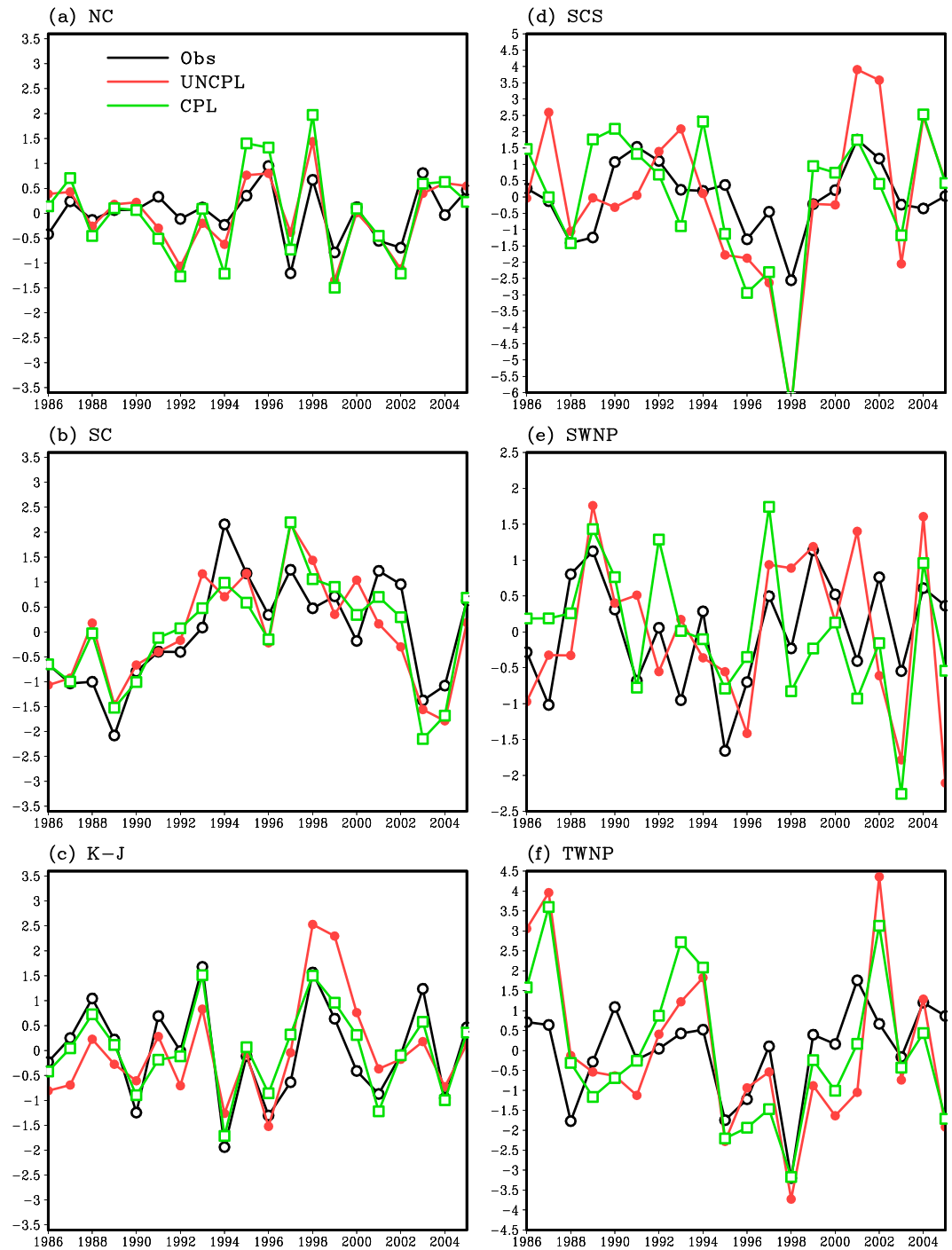
Figure 10. JJA precipitation anomaly (mm/day) over (a) northern part of China, (b) southern part of China, (c) Korea-Japan, (d) South China Sea, (e) subtropical western North Pacific, and (f) Tropical western North Pacific. Observation is in *black*, UNCPL is in *red*, and CPL is in *green*. JJA = June-July-August.

over SCS and the eastern coast offshore of the Philippines, while this positive precipitation bias in UNCPL is significantly alleviated in CPL. In addition, the UNCPL does not capture the observed northwest-southeast distribution of precipitation over TWNP, but this observed feature is reproduced in CPL. The difference between CPL and UNCPL is shown in Figure 6d, and the regions are hatched if the differences are statistically significance at 95% confidence level. Compared with the UNCPL, the CPL generates more

Table 3
The JJA Precipitation Anomaly Correlation of the UNCPL and CPL Against the Observation (GPCP Over Ocean, APHRODITE Over Land)

	NC	SC	K-J	SCS	SWNP	TWNP
UNCPL	0.70	0.72	0.70	**0.68**	0.34	0.50
CPL	**0.74**	**0.84**	**0.90**	0.67	**0.59**	**0.56**

Note. JJA = June-July-August; GPCP = Global Precipitation Climatology Project; APHRODITE = Asian Precipitation - Highly Resolved Observational Data Integration Towards Evaluation; NC = northern part of China; SC = southern part of China; K-J = Korea-Japan; SCS = South China Sea; SWNP = subtropical western North Pacific; TWNP = tropical western North Pacific. Values in bold indicate better results.

precipitation over the land areas and significantly less precipitation over the ocean. The overestimated precipitation over the ocean in the UNCPL is largely reduced in the CPL, indicating an improvement of precipitation simulation in the CPL. Without the air-sea interaction, the UNCPL overestimates the surface evaporation, and this subsequently causes the overestimation of precipitation over the ocean. The relationship of SST-evaporation will be discussed in detail in section 5.

Precipitation is closely linked with atmospheric circulation patterns and moisture availability. Figure 7 shows the JJA climatology of winds at 850 mb and moisture flux convergence at 1,000 mb. The rainfall bands and local maxima in Figure 6 are largely attributed to the strong moisture flux convergence at 1,000 mb. The precipitation bias in model simulations can also be explained by the model error in simulating winds at 850 mb. For example, the UNCPL generates a southwesterly-southeasterly wind convergent zone in the southeast part of the domain. This convergent zone is in near-zonal direction, where the observed convergent zone is in southeast-northwest direction. Subsequently, the UNCPL produces a near-zonal rainfall bands over the TWNP region but fails to produce the observed southeast-northwest oriented rainfall band.

The evolution of the monsoon precipitation can be examined in a Hovmoeller diagram. Figure 8 shows the monthly precipitation climatology averaged between 105°E and 140°E. There are two precipitation bands in observations: the northward tilt of the precipitation band in the north represents the northward propagation of the EASM from May to August; the other precipitation band is centered around 13°N (Figure 8a). In the UNCPL simulation, the northern band is nearly horizontal, and the amount of precipitation in the southern band is overestimated (Figure 8b). In the CPL simulation, the northern band is tilted northward from June to August, and the southern band is significantly alleviated compared with the UNCPL simulation (Figure 8c). The CPL improves the temporal evolution of precipitation, particularly the northward propagation of the EASM precipitation.

The JJA precipitation mean bias error and root-mean-square error (RMSE) over the six regions are listed in Table 2. In NC, the UNCPL underestimates the mean precipitation, and the CPL overestimates the mean precipitation. Compared to the UNCPL, the CPL has smaller errors in both measurements. In SC, the UNCPL slightly overestimates the mean precipitation, and the CPL underestimates the mean precipitation. Compared to the UNCPL, the CPL has smaller RMSE. In K-J, both UNCPL and CPL underestimate the mean precipitation, and the RMSE is larger than that over the land regions of NC and SC. In both SCS and SWNP, the UNCPL largely overestimates the mean precipitation and has a high value of RMSE. Both mean bias error and RMSE in the CPL are significantly reduced. In TWNP, the UNCPL overestimates the mean precipitation, and the CPL underestimates the mean precipitation. Compared to the UNCPL, the CPL has smaller RMSE.

4.2. Interannual Variability

The pointwise correlation of JJA precipitation between model simulation and observation is shown in Figure 9. The correlation between observation and UNCPL is 0.40 over the land and is 0.36 over the ocean, while the correlation between observation and CPL is 0.42 over the land and 0.44 over the ocean. The correlation difference between CPL and UNCPL is shown in Figure 9c, and the regions are hatched if the differences are statistically significance at 95% confidence level (Siegert et al., 2017). It is evident that the CPL improved precipitation simulation, particularly over K-J, SCS, SWNP, and TWNP.

The JJA precipitation anomalies over the six regions are shown in Figure 10, and anomaly correlation coefficients (ACCs) between the observed and simulated JJA precipitation are listed in Table 3. In NC and SC regions, the year-to-year variation of JJA precipitation in UNCPL and CPL generally agrees with the observation (Figures 10a and 10b). The correlation of JJA precipitation is statistically significant at 95% confidence level in both UNCPL and CPL, and the ACC is higher in CPL, compared to the UNCPL. In K-J region, the correlation of JJA precipitation is statistically significant at 95% confidence level in both UNCPL and CPL. Compared to the UNCPL, the CPL has a higher value of ACC. This is largely attributed to a better simulation of CPL during 1986–1990 (Figure 10c).
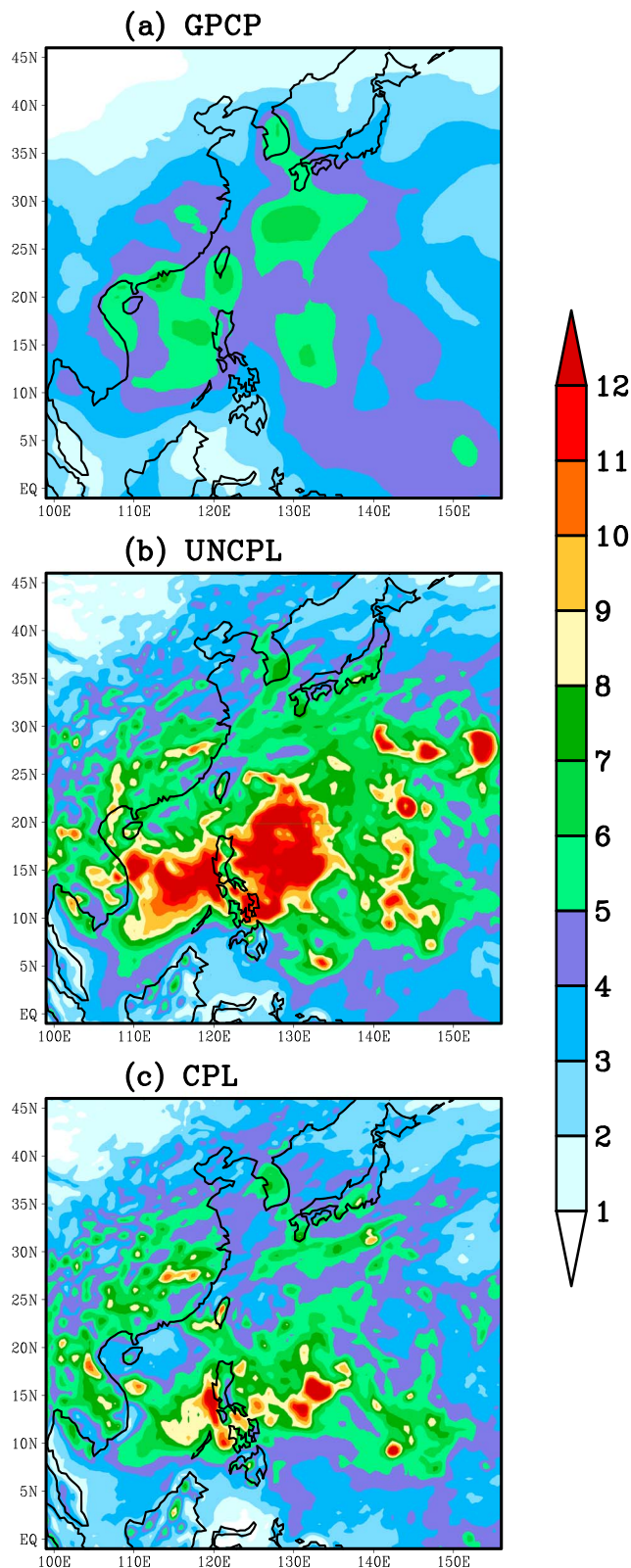
Figure 11. The 20- to 90-day bandpass-filtered precipitation variance (mm/day) for JJA during 1997–2005 from (a) GPCP observation, (b) UNCPL and (c) CPL. GPCP = Global Precipitation Climatology Project; JJA = June-July-August.

In SCS region, the correlation of JJA precipitation is statistically significant at 95% confidence level in both UNCPL and CPL. Although the ACC values are close to each other, the UNCPL and CPL exhibit different year-to-year variation during 1986–1994 (Figure 10d). In SWNP region, the correlation of JJA precipitation is statistically significant at 95% confidence level in CPL only. The low value of ACC in UNCPL can be explained by the poor simulation of UNCPL in Figure 10e. In TWNP region, the correlation of JJA precipitation is statistically significant at 95% confidence level in both UNCPL and CPL, and the ACC is higher in CPL, compared to the UNCPL.

In general, both the UNCPL and CPL simulate the interannual variability of JJA precipitation better over the land (i.e., NC, SC, and K-J) than the ocean (i.e., SCS, SWNP, and TWNP). The correlation difference between CPL and UNCPL in Table 3 is statistically significant at 95% confidence level (Siegert et al., 2017) over SC and K-J, indicating the improvement on interannual variability of precipitation over SC and K-J in the CPL.

4.3. Intraseasonal Variability

The intraseasonal variability of JJA precipitation is examined in this section. We use the period of 1997–2005 for verification due to the availability of observed daily data. The variance of daily precipitation filtered with a 20- to 90-day bandpass is shown in Figure 11. Strong intraseasonal variability is observed over the ocean, coastal regions of China, and the K-J region (Figure 11a). The intraseasonal variance in the UNCPL is much stronger than that in observations (Figure 11b), especially over the ocean. The unrealistic strong intraseasonal variance is alleviated in the CPL (Figure 11c). The CPL captures the spatial characteristics of observed intraseasonal variance, although the variance in CPL is generally stronger compared with observations.

5. Discussion

In order to confirm the importance of the atmosphere-ocean coupling, the coupling issue is isolated and examined through a perfect model experiment: the RSM is forced with the daily SST from CPL (SSTCPL hereafter). We find out that SSTCPL has similar performance in simulating the climatology (Figure 12a), intraseasonal variability (Figure 12b), and interannal variability of EASM precipitation as CPL (not shown). This result provides clear evidence that the SST-forced response in the coupled and uncoupled simulations is the same and further suggests that the difference between UNCPL and CPL is due to lack of coupling to the ocean rather than atmospheric model bias unrelated to coupling. The relationship between boreal summer SST and precipitation (evaporation) is discussed as below.

5.1. The Relationship Between Boreal Summer SST and Precipitation

The results in section 4 show that the simulation of EASM precipitation is improved in the CPL compared to UNCPL, which is forced by observed SST. It is natural to examine the relationship between boreal summer SST and precipitation in model simulations. The pointwise correlation of JJA SST and precipitation is shown in Figure 13. Observations exhibit negative correlations over most of the domain (Figure 13a). The negative correlation is statistically significant at 95% confidence level over the SCS, the Yellow Sea, the Sea of Japan, the southern Japan offshore area, the eastern Taiwan offshore area, the Philippine Sea, and the TWNP. This result is consistent with previous studies (Cha et al., 2016; Wang et al., 2004; Wu &
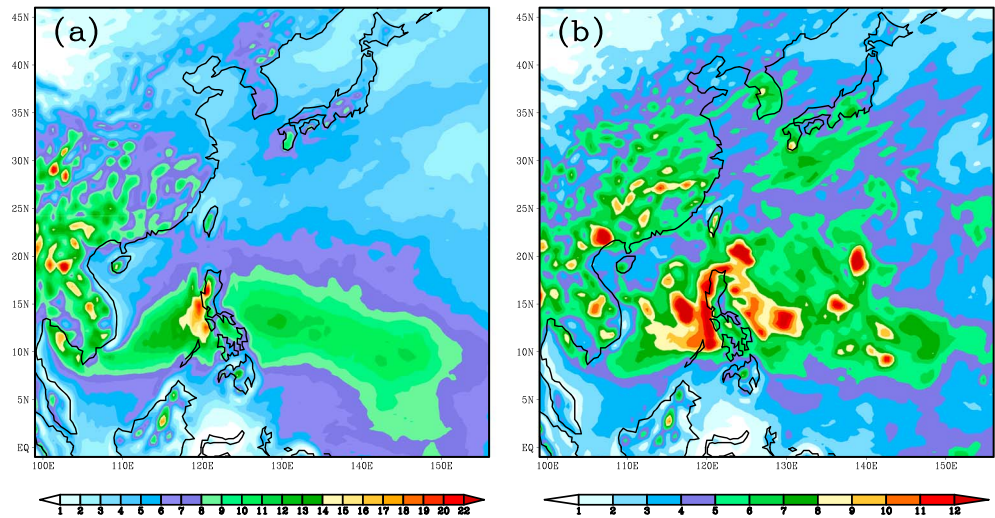
Figure 12. (a) JJA precipitation climatology (mm/day) from SSTCPL. (b) The 20- to 90-day bandpass-filtered precipitation variance (mm/day) for JJA during 1997–2005 from SSTCPL. JJA = June-July-August; SSTCPL = SST from CPL.

Kirtman, 2007). In the UNCPL simulation, the negative correlation is weak and is not statistically significant at 95% confidence level over the Sea of Japan and SCS. The positive correlations over SWNP are also not consistent with observations, indicating an unrealistic fast response of atmosphere to SST forcings in UNCPL (Figure 13b). Strong negative correlations in the observations are captured by the CPL, although the area with negative correlation is a little bigger than that in the observations (Figure 13c).
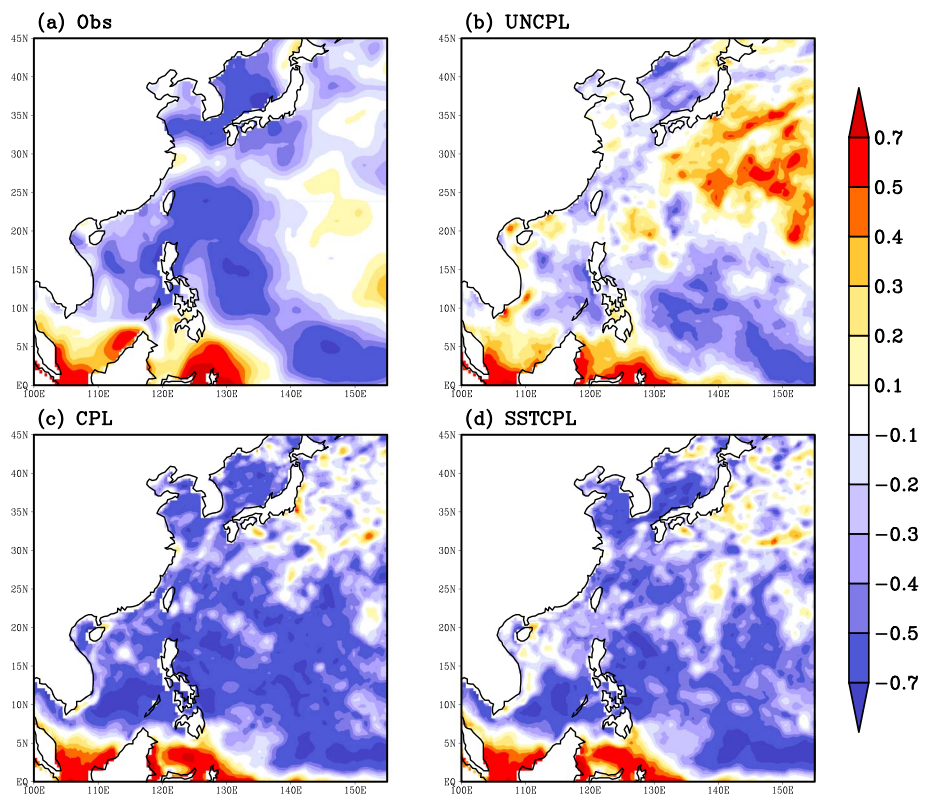

Figure 13. Correlation coefficients between the JJA SST and precipitation for the period of 1986–2005 from (a) observation, (b) UNCPL, (c) CPL, and (d) SSTCPL. JJA = June-July-August; SSTCPL = SST from CPL; SST = sea surface temperature.
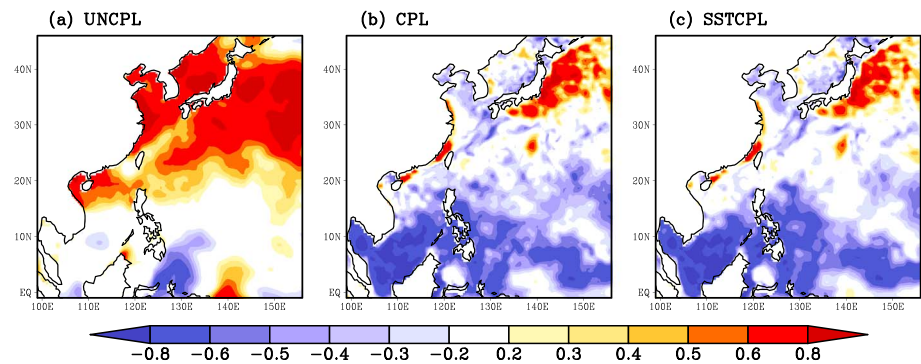
Figure 14. Correlation coefficients between the JJA SST and evaporation for the period of 1986–2005 from (a) UNCPL, (b) CPL, and (c) SSTCPL. JJA = June-July-August; SSTCPL = SST from CPL; SST = sea surface temperature.

In the experiment of UNCPL, SST anomalies are the local external boundary forcing and the atmosphere can only passively respond to SST forcings. However, the SST and precipitation interact with each other over the EASM region, and the SST anomalies are largely a response to the atmospheric monsoon forcing (Wang et al., 2004). The SST-precipitation relationship is more realistically presented in the CPL, which includes the two-way ocean-atmosphere interactions. The increased precipitation and cloudiness tend to reduce the downward solar radiation into the ocean mixed layer. Simultaneously, the increased precipitation intensifies the low-level monsoon westerly winds, which further intensifies the surface evaporation cooling and the entrainment cooling of the mixed layer. Furthermore, positive surface wind stress curl corresponds to the increased precipitation, and this would raise the thermocline through Ekman pumping in the upper ocean, which would also cool the local SSTs (Cha et al., 2016; Wang et al., 2004). The SSTCPL (Figure 13d) also resembles the pattern from CPL (Figure 13c).

5.2. The Relationship Between Boreal Summer SST and Evaporation

The surface evaporation plays an important role in air-sea interactions, and it is useful to identify the local coupling from the relationship between SST and surface evaporation (Barsugli & Battisti, 1998; Wu & Kirtman, 2007). The pointwise correlation of JJA SST and evaporation (Figure 14) is calculated to further reveal the air-sea interaction regime over the EASM region. Negative correlations are only over southern SCS and the offshore in southeast Philippines, and positive correlations prevail over all other regions from the UNCPL (Figure 14a). The positive correlation indicates the dominance of oceanic forcing to the atmosphere over EASM in UNCPL. The CPL displays the feature of SST-evaporation relationship quite differently: negative correlations are prevailing over SCS, SWNP, and TWNP from CPL, and positive correlations are along the coastline of China and over the east Japan offshore area (Figure 14b). This is consistent with previous studies (e.g., Wu & Kirtman, 2007). The prevailing negative SST-evaporation correlation indicates the dominance of atmospheric forcing to the ocean over EASM region in the CPL. The SSTCPL (Figure 14c) also reproduces the SST-evaporation relationship in CPL.

6. Summary and Conclusions

In this study, a 22-year climate simulation of EASM was done with a regional ocean-atmosphere coupled model (RSM-ROMS), forced by the National Centers for Environmental Prediction-Department of Energy global atmospheric reanalysis and SODA oceanic reanalysis. Note that a climatology heat flux correction was applied during this coupled integration. The horizontal grid resolution is approximately 40 km, and the domain covers the EASM region (5.415°S–50.334°N, 92.725°E–164.245°E). The impact of local air-sea interaction on EASM precipitation is examined in CPL and compared with UNCPL forced with observed SST. A series in situ and satellite observations are used to examine the simulation of UNCPL and CPL.

The surface oceanic features are well simulated in CPL: The observed Kuroshio Current and the variability of SSH are captured in CPL. The CPL also reproduced the observed summer SST climatology and the interannual variability. A cold bias around 0.5 °C is found over SWNP, possibly attributed to the excessive cloud cover in the CPL simulation. The temporal correlation of CPL-simulated JJA SST against observation is 0.87 over SCS.

The variation of SST from CPL is much smaller than observations over SWNP, although the correlation coefficient is 0.80 over SWNP. The SST variability from CPL matches the observation well over TWNP, and the correlation is as high as 0.95.

The evaluation of EASM precipitation is the core of this study. Both UNCPL and CPL can generate a northeastward rainfall band over SC, the Yangtze River basin, Korea, and Japan but underestimate the precipitation over K-J. The UNCPL overestimates precipitation over SCS and the offshore area of the eastern Philippines, and the positive precipitation bias in UNCPL is significantly reduced in CPL.

The evolution of the monsoon precipitation was examined in a Hovmoeller diagram. There are two precipitation bands in observations: the northward tilt of the precipitation band in the north represents the northward propagation of the EASM from May to August; the other precipitation band is centered around 13°N. In the UNCPL simulation, the northern band is nearly horizontal, and the amount of precipitation in the southern band is overestimated. In the CPL simulation, the northern band is tilted northward from June to August, and the southern band is significantly alleviated compared with the UNCPL simulation. The CPL improves the temporal evolution of precipitation, particularly the northward propagation of the EASM precipitation.

The anomaly correlation between the observed and simulated JJA precipitation is statistically significant at 95% confidence level over all regions except for the SWNP in the UNCPL simulation. The CPL is better than UNCPL in simulation of JJA precipitation and its interannual variability over SC, K-J, and SWNP with statistically significance at 95% confidence level.

The pointwise correlation of JJA SST and precipitation is used to examine the boreal summer SST-precipitation relationship. The CPL shows negative correlation over most of the domain, which is consistent with the observations. The negative correlation is statistically significant at 95% confidence level over the SCS, the Yellow Sea, the Sea of Japan, the southern Japan offshore area, the eastern Taiwan offshore area, the Philippine Sea, and the TWNP. However, UNCPL shows weaker negative correlations over the Sea of Japan, the SCS, and the Philippine Sea, compared to the CPL. UNCPL also show positive correlations over SWNP, which is not consistent with observations. Therefore, the CPL is better than UNCPL in simulation of the SST-precipitation relationship. The pointwise correlation between SST and evaporation is used to further reveal the air-sea interaction of EASM. The UNCPL and CPL show quite different air-sea coupling mechanism during EASM. The dominant positive SST-evaporation correlation indicates the dominance of SST forcing of atmosphere in UNCPL, while the prevailing negative SST-evaporation correlation indicates the dominance of atmosphere forcing to the ocean in CPL. The SSTCPL, in which RSM is forced by the daily SST from CPL, well resembles the SST-precipitation and SST-evaporation relationship as CPL. This further confirms the impact of air-sea interaction for EASM precipitation.

This study shows that a fully coupled regional ocean-atmosphere model is able to represent the air-sea interaction during EASM. The climatology, interannual, and intraseasonal variations of EASM precipitation are improved in CPL compared with the UNCPL, which is forced with the prescribed SST. It indicates that a fully regional ocean-atmosphere coupled model is essential for the simulation of EASM precipitation.

References

Alpert, J. C., Kanamitsu, M., Caplan, P. M., Sela, J. G., White, G. H., & Kalnay, E. (1988). Mountain induced gravity wave drag parameterization in the NMC medium-range model. In *Preprints, Eighth Conf. on Numerical Weather Prediction* (pp. 726–733). Baltimore, MD: American Meteorology Society.

Barsugli, J. J., & Battisti, D. S. (1998). The basic effects of atmosphere-ocean thermal coupling on midlatitude variability. *Journal of the Atmospheric Sciences*, 55(4), 477–493. https://doi.org/10.1175/1520-0469(1998)055<0477:TBEOAO>2.0.CO;2

Bonjean, F., & Lagerloef, G. S. E. (2002). Diagnostic model and analysis of the surface currents in the tropical Pacific Ocean. *Journal of Physical Oceanography*, 32, 2938–2954. https://doi.org/10.1175/1520-0485(2002)032<2938:DMAAOT>2.0.CO;2

Carton, J. A., Chepurin, G., Cao, X., & Giese, B. (2000). A Simple Ocean Data Assimilation analysis of the global upper ocean 1950–1995. Part I: Methodology. *Journal of Physical Oceanography*, 30(2), 294–309. https://doi.org/10.1175/1520-0485(2000)030<0294:ASODAA>2.0.CO;2

Cha, D.-H., Jin, C.-S., Moon, J.-H., & Lee, D.-K. (2016). Improvement of regional climate simulation of East Asian summer monsoon by coupled air-sea interaction and large-scale nudging. *International Journal of Climatology*, 36(1), 334–345. https://doi.org/10.1002/joc.4349

Chou, M.-D., & Lee, K.-T. (1996). Parameterizations for the absorption of solar radiation by water vapor and ozone. *Journal of the Atmospheric Sciences*, 53(8), 1203–1208. https://doi.org/10.1175/1520-0469(1996)053<1203:PFTAOS>2.0.CO;2

Chou, M.-D., & Suarez, M.-J. (1994). An efficient thermal infrared radiation parameterization for use in general circulation models. Technical report series on global modeling and data assimilation, NASA/TM-1994-104606, 3 (85 pp.).

Ding, Y.-H., & Chan, J. C. L. (2005). The East Asian summer monsoon: An overview. *Meteorology and Atmospheric Physics*, 89(1-4), 117–142. https://doi.org/10.1007/s00703-005-0125-z

Ek, M. B., Mitchell, K. E., Lin, Y., Rogers, E., Grunmann, P., Koren, V., et al. (2003). Implementation of Noah land surface model advances in the National Centers for Environmental Prediction operational mesoscale Eta model. *Journal of Geophysical Research*, *108*(D22), 8851. https://doi.org/10.1029/2002JD003296

Fang, Y., Zhang, Y., Tang, J., & Ren, X. (2010). A regional air-sea coupled model and its application over East Asia in the summer of 2000. *Advances in Atmospheric Sciences*, *27*(3), 583–593. https://doi.org/10.1007/s00376-009-8203-7

Fasham, M. J. R., Ducklow, H. W., & McKelvie, S. M. (1990). A nitrogen-based model of plankton dynamics in the ocean mixed layer. *Journal of Marine Research*, *48*(3), 591–639. https://doi.org/10.1357/002224090784984678

Fearing, A. L., Donohue, K. A., & Watts, D. R. (2006). Sea surface height variability in the Kuroshio extension. SURFO Technical Report No. 2006-02, 22–25.

Fisher, M. (1998). Minimization algorithms for variational data assimilation. In *Recent Developments in Numerical Methods for Atmospheric Modelling* (pp. 364–385). Shinfield Park, Reading: ECMWF Publication.

Gorgi, F., & Gao, X. (2018). Regional earth system modeling: Review and future directions. *Atmospheric and Oceanic Science Letters*, *11*(2), 189–197. https://doi.org/10.1080/16742834.2018.1452520

Haidvogel, D. B., Arang, H. G., Hedstrom, K., Beckmann, A., Malanotte-Rizzoli, P., & Shchepetkin, A. F. (2000). Model evaluation experiments in the North Atlantic Basin: Simulations in nonlinear terrain-following coordinates. *Dynamics of Atmospheres and Oceans*, *32*(3-4), 239–281. https://doi.org/10.1016/S0377-0265(00)00049-X

Haidvogel, D. B., & Beckmann, A. (1999). *Numerical ocean circulation modeling*. London: Imperial College Press.

Ham, S., Yoshimura, K., & Li, H. (2016). Historical dynamical downscaling for East Asia with the atmosphere and ocean coupled regional model. *Journal of the Meteorological Society of Japan*, *94A*, 199–208. https://doi.org/10.2151/jmsj.2015-046

Hong, S.-Y., & Pan, H.-L. (1996). Nonlocal boundary layer vertical diffusion in a medium-range forecast model. *Monthly Weather Review*, *124*(10), 2322–2339. https://doi.org/10.1175/1520-0493(1996)124<2322:NBLVDI>2.0.CO;2

Huffman, G. J., Adler, R. F., Arkin, P., Chang, A., Ferraro, R., Gruber, A., et al. (1997). The global precipitation climatology project (GPCP) combined precipitation dataset. *Bulletin of the American Meteorological Society*, *78*(1), 5–20. https://doi.org/10.1175/1520-0477(1997)078<0005:TGPCPG>2.0.CO;2

Huffman, G. J., Alder, R. F., Morrissey, M., Bolvin, D. T., Curtis, S., Joyce, R., et al. (2001). Global precipitation at one-degree daily resolution from multi-satellite observation. *Journal of Hydrometeorology*, *2*(1), 36–50. https://doi.org/10.1175/1525-7541(2001)002<0036:GPAODD>2.0.CO;2

Juang, H.-M., Hong, S.-Y., & Kanamitsu, M. (1997). The NCEP regional spectral model: An update. *Bulletin of the American Meteorological Society*, *78*(10), 2125–2143. https://doi.org/10.1175/1520-0477(1997)078<2125:TNRSMA>2.0.CO;2

Juang, H.-M., & Kanamitsu, M. (1994). The NMC nested regional spectral model. *Monthly Weather Review*, *122*(1), 3–26. https://doi.org/10.1175/1520-0493(1994)122<0003:TNNRSM>2.0.CO;2

Kain, J. S. (2004). The Kain-Fritsch Convective Parameterization: An Update. *Journal of Applied Meteorology*, *43*, 170–181. https://doi.org/10.1175/1520-0450(2004)043<0170:TKCPAU>2.0.CO;2

Kanamaru, H., & Kanamitsu, M. (2007). Scale-selective bias correction in a downscaling of global reanalysis using a regional model. *Monthly Weather Review*, *135*(2), 334–350. https://doi.org/10.1175/MWR3294.1

Kanamitsu, M., Ebisuzaki, W., Woollen, J., Yang, S.-K., Hnilo, J. J., Fiorino, M., & Potter, G. L. (2002). NCEP-DOE AMIP-II reanalysis (R-2). *Bulletin of the American Meteorological Society*, *83*(11), 1631–1644. https://doi.org/10.1175/BAMS-83-11-1631

Kanamitsu, M., Yoshimura, K., Yhang, Y., & Hong, S.-Y. (2010). Errors of interannual variability and multi-decadal trend in dynamical regional climate downscaling and its corrections. *Journal of Geophysical Research*, *115*, D17115. https://doi.org/10.1029/2009JD013511

Kim, E.-J., & Hong, S.-Y. (2010). Impact of air-sea interaction on East Asian summer monsoon climate in WRF. *Journal of Geophysical Research*, *115*, D19118. https://doi.org/10.1029/2009JD013253

Large, W. G., McWilliams, J. C., & Doney, S. C. (1994). Oceanic vertical mixing: A review and a model with a nonlocal boundary layer para-meterization. *Reviews of Geophysics*, *32*, 363–403. https://doi.org/10.1029/94RG01872

Li, H., Kanamitsu, M., & Hong, S.-Y. (2012). California reanalysis downscaling at 10 km using an ocean-atmosphere coupled regional model system. *Journal of Geophysical Research*, *117*, D12118. https://doi.org/10.1029/2011JD017372

Li, H., Kanamitsu, M., Hong, S.-Y., Yoshimura, K., Cayan, D. R., & Misra, V. (2014). A high-resolution ocean-atmosphere coupled downscaling of a present climate over California. *Climate Dynamics*, *42*(3-4), 701–714. https://doi.org/10.1007/s00382-013-1670-7

Li, H., Kanamitsu, M., Hong, S.-Y., Yoshimura, K., Cayan, D. R., Misra, V., & Sun, L. (2014). Projected climate change scenario over California by a regional ocean-atmosphere coupled model system. *Climatic Change*, *122*(4), 609–619. https://doi.org/10.1007/s10584-013-1025-8

Li, H., & Misra, V. (2014). Thirty-two-year ocean-atmosphere coupled downscaling of global reanalysis over the Intra-American Seas. *Climate Dynamics*, *43*(9-10), 2471–2489. https://doi.org/10.1007/s00382-014-2069-9

Marchesiello, P., McWilliams, J. C., & Shchepetkin, A. (2001). Open boundary conditions for long-term integration of regional oceanic models. *Ocean Modelling*, *3*(1-2), 1–20. https://doi.org/10.1016/S1463-5003(00)00013-5

Ren, X., & Qian, Y. (2005). A coupled regional air-sea model, its performance and climate drift in simulation of the East Asian summer monsoon in 1998. *International Journal of Climatology*, *25*(5), 679–692. https://doi.org/10.1002/joc.1137

Reynolds, R. W., Smith, T. M., Liu, C., Chelton, D. B., Casey, K. S., & Schlax, M. G. (2007). Daily high-resolution-blended analyses for sea surface temperature. *Journal of Climate*, *20*, 5473–5496. https://doi.org/10.1175/2007JCLI1824.1

Rossow, W. B., & Schiffer, R. A. (1999). Advances in understanding clouds from ISCCP. *Bulletin of the American Meteorological Society*, *80*(11), 2261–2287. https://doi.org/10.1175/1520-0477(1999)080<2261:AIUCFI>2.0.CO;2

Sakamoto, T. T., Hasumi, H., Ishii, M., Emori, S., Suziki, T., Nishimura, T., & Sumi, A. (2005). Responses of the Kuroshio and Kuroshio extension to global warming in a high-resolution climate model. *Geophysical Research Letters*, *32*, L14617. https://doi.org/10.1029/2005GL023384

Shchepetkin, A. F., & McWilliams, J. C. (1998). Quasi-monotone advection schemes based on explicit locally adaptive dissipation. *Monthly Weather Review*, *126*(6), 1541–1580. https://doi.org/10.1175/1520-0493(1998)126<1541:QMASBO>2.0.CO;2

Shchepetkin, A. F., & McWilliams, J. C. (2003). A method for computing horizontal pressure-gradient force in an oceanic model with a non-aligned vertical coordinate. *Journal of Geophysical Research*, *108*(C3), 3090. https://doi.org/10.1029/2001JC001047

Siegert, S., Bellprat, O., Ménégoz, M., Stephenson, D. B., & Doblas-Reyes, F. J. (2017). Detecting improvements in forecast correlation skill: Statistical testing and power analysis. *Monthly Weather Review*, *145*(2), 437–450. https://doi.org/10.1175/MWR-D-16-0037.1

Slingo, J. M. (1987). The development and verification of a cloud prediction model for the ECWMF model. *Quarterly Journal of the Royal Meteorological Society*, *113*(477), 899–927. https://doi.org/10.1002/qj.49711347710

Song, F., & Zhou, T. (2014). The climatology and interannual variability of East Asian summer monsoon in CMIP5 coupled models: Does air-sea coupling improve the simulations? *Journal of Climate*, *27*(23), 8761–8777. https://doi.org/10.1175/JCLI-D-14-00396.1

Song, Y.-T., & Haidvogel, D. B. (1994). A semi-implicit ocean circulation model using a generalized topography following coordinate system. *Journal of Computational Physics*, *115*(1), 228–244. https://doi.org/10.1006/jcph.1994.1189

Tiedtke M., (1983). The sensitivity of the time-mean large-scale flow to cumulus convection in the ECMWF model. Proc. ECMWF Workshop on Convective in Large-Scale Models, Reading, United Kingdom, European Centre for Medium-Range Weather Forecasts (pp. 297–316).

Wang, B., Kang, I.-S., & Lee, J.-Y. (2004). Ensemble simulation of Asian-Australian monsoon variability by 11 AGCMs. *Journal of Climate*, *17*, 803–818. https://doi.org/10.1175/1520-0442(2004)017<0803:ESOAMV>2.0.CO;2

Wu, R., & Kirtman, B. P. (2007). Regimes of seasonal air-sea interaction and implications for performance of forced simulations. *Climate Dynamics*, *29*(4), 393–410. https://doi.org/10.1007/s00382-007-0246-9

Yatagai, A., Kamiguchi, K., Arakwawa, O., Hamada, A., Yasutomi, N., & Kitoh, A. (2012). APHRODITE: Constructing a long-term daily gridded precipitation dataset for Asia based on a dense network of rain gauges. *Bulletin of the American Meteorological Society*, *93*(9), 1401–1415. https://doi.org/10.1175/BAMS-D-11-00122.1

Zhou, T., Wu, B., & Wang, B. (2009). How well do atmospheric general circulation models capture the leading modes of the interannual variability of the Asian-Australian monsoon? *Journal of Climate*, *22*(5), 1159–1173. https://doi.org/10.1175/2008JCLI2245.1

Zou, L., & Zhou, T. (2013). Can a regional ocean-atmosphere coupled model improve the simulation of the interannual variability of the western North Pacific summer monsoon? *Journal of Climate*, *26*(7), 2353–2367. https://doi.org/10.1175/JCLI-D-11-00722.1